

Article

Multifiltering Algorithm for Enhancing the Accuracy of Individual Tree Parameter Extraction at *Eucalyptus* Plantations Using LiDAR Data

Jinjun Huang , Wen He and Yuefeng Yao *

Guangxi Institute of Botany, Guangxi Zhuang Autonomous Region and Chinese Academy of Sciences, Guilin 541006, China; jinjun.h@gxib.cn (J.H.); hw@gxib.cn (W.H.)

* Correspondence: yf.yao@gxib.cn

Abstract: Accurately quantifying individual tree parameters is a critical step for assessing carbon sequestration in forest ecosystems. However, it is challenging to gather comprehensive tree point cloud data when using either unmanned aerial vehicle light detection and ranging (UAV-LiDAR) or terrestrial laser scanning (TLS) alone. Moreover, there is still limited research on the effect of point cloud filtering algorithms on the extraction of individual tree parameters from multiplatform LiDAR data. Here, we employed a multifiltering algorithm to increase the accuracy of individual tree parameter (tree height and diameter at breast height (DBH)) extraction with the fusion of TLS and UAV-LiDAR (TLS-UAV-LiDAR) data. The results showed that compared to a single filtering algorithm (improved progressive triangulated irregular network densification, IPTD, or a cloth simulation filter, CSF), the multifiltering algorithm (IPTD + CSF) improves the accuracy of tree height extraction with TLS, UAV-LiDAR, and TLS-UAV-LiDAR data (with R^2 improvements from 1% to 7%). IPTD + CSF also enhances the accuracy of DBH extraction with TLS and TLS-UAV-LiDAR. In comparison to single-platform LiDAR (TLS or UAV-LiDAR), TLS-UAV-LiDAR can compensate for the missing crown and stem information, enabling a more detailed depiction of the tree structure. The highest accuracy of individual tree parameter extraction was achieved using the multifiltering algorithm combined with TLS-UAV-LiDAR data. The multifiltering algorithm can facilitate the application of multiplatform LiDAR data and offers an accurate way to quantify individual tree parameters.

Keywords: individual tree parameter; point cloud filtering algorithm; LiDAR; terrestrial laser scanning (TLS); unmanned aerial vehicles (UAV)



Citation: Huang, J.; He, W.; Yao, Y. Multifiltering Algorithm for Enhancing the Accuracy of Individual Tree Parameter Extraction at *Eucalyptus* Plantations Using LiDAR Data. *Forests* **2024**, *15*, 81. <https://doi.org/10.3390/f15010081>

Academic Editor: Alfonso Fernández-Manso

Received: 26 November 2023
Revised: 21 December 2023
Accepted: 26 December 2023
Published: 30 December 2023



Copyright: © 2023 by the authors. Licensee MDPI, Basel, Switzerland. This article is an open access article distributed under the terms and conditions of the Creative Commons Attribution (CC BY) license (<https://creativecommons.org/licenses/by/4.0/>).

1. Introduction

Vegetation structural parameters, as the most crucial explanatory variables for investigating the dynamic changes in forest ecosystems, play a critical role in predicting carbon and water cycles in terrestrial ecosystems [1]. The accurate quantification of individual tree parameters can support the development of high-quality forest ecological environments [2]. It is also essential to understand how forest ecosystems respond to climatic and environmental variations. Rapid progress in remote sensing technology has effectively mitigated the constraints associated with traditional manual surveys, enabling the swift and convenient monitoring of large-scale forest dynamics [3,4]. Light detection and ranging (LiDAR) technology uses laser pulses to obtain three-dimensional information about target objects, providing the advantage of rapidly acquiring vertical vegetation structure parameters, benefits that cannot be matched by optical remote sensing [5–7].

LiDAR can be further classified into two categories: airborne LiDAR and ground-based LiDAR, depending on the platform and operation mode [8]. The use of unmanned aerial vehicles (UAVs) has further promoted its application in forestry research, owing to flexible route planning, operational simplicity, and the ability to provide high-spatial-resolution data [9]. Remotely Piloted Aircraft Systems (RPASs) [10] equipped with LiDAR

sensors offer advanced and reliable tools for forest resource management and ecosystem research, advancing the understanding of forest vegetation conditions. In recent years, UAV-LiDAR and terrestrial laser scanning (TLS) have been widely applied to extract vegetation structural parameters [11–13]. The top-down scanning approach of UAV-LiDAR easily gathers information about forest canopies and has been applied in extensive forest inventories [14]. However, UAV-LiDAR struggles to accurately capture stem information beneath the canopy. In contrast, TLS can be used to nondestructively measure understory vegetation [15]. Nevertheless, TLS encounters issues with occlusion when measuring canopy and subcanopy structures. To overcome this problem, multistation scanning or dynamic scanning can be employed to collect TLS data. Liu et al. [16] noted that multistation terrestrial point clouds could yield more accurate results than single-station point clouds.

The individual tree parameters of tree height and diameter at breast height (DBH) are critical growth metrics for trees. UAV-LiDAR can accurately measure tree height, while TLS relies on its higher scanning density to obtain an accurate DBH. The distinct characteristics of multiplatform LiDAR data underscore the necessity for a comparative analysis of individual tree parameter estimates [17]. While UAV-LiDAR tends to depict the upper canopy structure, TLS focuses on the lower portion of the canopy. However, it is evident that the fusion of UAV-LiDAR and TLS has the potential to reduce shading and improve the accuracy of quantifying forest structure metrics [18]. Many scholars have strived to fuse multiplatform LiDAR to overcome the limitations of single-platform LiDAR in parameter estimation. Fekry et al. [19] fused UAV-LiDAR and TLS data for quantitative structural modelling and tree parameter inversion in subtropical plantation forests. Dimitrios et al. [20] fused UAV-LiDAR and TLS data to evaluate the managed temperate forest structure.

Many efforts have been devoted to developing tree segmentation algorithms for improving the accuracy of individual tree parameter extraction [21,22]. Point cloud filtering is performed as an essential step in the postprocessing of LiDAR data [23,24]. This process can separate ground points from nonground points, which can also improve the accuracy of individual tree parameter extraction. However, there is connectivity between ground points and tree structure point clouds [25], making it impossible to extract tree information directly with segmentation algorithms.

Many algorithms have been proposed to automatically filter ground points [26–28]. Compared to traditional progressive triangulated irregular network (TIN) algorithms, the improved progressive TIN densification (IPTD) overcomes the issue of uneven seed point distribution by employing morphological windowing [29]. This provides a more accurate point cloud of the terrain. However, it is time consuming to obtain a large number of uniformly distributed ground points with IPTD. The cloth simulation filter (CSF) algorithm has been gradually gaining attention due to its easy-to-set parameters and adaptive strength [30]. Compared with IPTD, the CSF has higher computational efficiency. However, the CSF heavily relies on fixed position points and may not be able to produce ideal ground points in complex terrain. Therefore, combining the IPTD and CSF algorithms may significantly increase the ground point separation accuracy.

Eucalyptus spp. are among the most widely planted species due to their fast growth rate [31]. In China, especially in Guangxi Zhuang Autonomous Region, the planted area of *Eucalyptus* plantations has expanded to over 1.8 million hectares in the past decade [32]. Effectively utilizing LiDAR data from different platforms to obtain accurate individual tree parameters is crucial for the efficiency of monitoring and managing forest resources at plantations [33]. This study focuses on individual tree parameter extraction from different-aged *Eucalyptus* plantations based on TLS, UAV-LiDAR, and TLS-UAV-LiDAR data in the subtropical region of southern China. The objectives were (1) to explore the potential of extracting individual tree parameters with TLS, UAV-LiDAR, and TLS-UAV-LiDAR data; and (2) to combine IPTD and the CSF (IPTD + CSF) and compare the performance of this approach in individual tree parameter extraction with that of the IPTD and CSF algorithms alone using multiplatform LiDAR data.

2. Materials and Methods

2.1. Study Area

The study area was located in the transitional region from the South Asian tropical zone to the Central Asian tropical zone, specifically within the state-owned Huangmian Forest Farm, Guangxi Zhuang Autonomous Region, China. This area is mainly characterized by hilly terrain, with a general trend of higher elevation in the northeast and lower elevation in the southwest. The soil is predominantly yellowish-red soil with a high clay content. The annual average temperature is approximately 20 °C and the annual average rainfall ranges from 1750 to 2000 mm. The vegetation is mainly composed of *Eucalyptus* spp. and *Cunninghamia lanceolata* (Lamb.) Hook, with interspersed species such as *Schima superba* Gardn. et Champ, *Michelia macclurei* Dandy, and *Phyllostachys heterocycla* (Carr.) Mitford cv. Pubescens.

2.2. Data Collection

Field measurements were obtained in November 2022. Standard plots of 20 m × 20 m were established in six different ages of *Eucalyptus* plantations, which were planted annually from 2016 to 2021. Information such as the slope, aspect, elevation, and stand density of each plot was recorded. Each tree within the plots was measured, and data from a total of 307 trees were collected. A TruPulse200 laser rangefinder (Laser Technology Inc., Centennial, CO, USA) was used to measure the tree height. Each tree was measured three times, and the average value was used as the final tree height. All trees with a DBH greater than 5 cm were measured. When setting up plots, careful consideration was given to signal reception from the Real-Time Kinematic (RTK) system. Measurements were conducted under clear weather conditions with minimal ionospheric disturbance. Tree and plot corner coordinates were obtained using the Hi-Target D8pro (Satellite Navigation Technology Co., Ltd., Guangzhou, China), with a horizontal positioning accuracy of ±8 mm. To ensure precision, the pole was positioned as close to the base of the tree as possible, maintaining a fixed solution state (horizontal tolerance of ±0.02 m and vertical tolerance of ±0.05 m). For plots with weak signals, an alternative approach involved using a 1 + 1 mode. In this mode, a base station was placed in an open area around the sample plot to receive signals, while another station served as a mobile station for point positioning.

TLS data were collected with a Faro Focus 3D device (Faro Technologies Inc., Lake Mary, FL, USA) within one selected 20 m × 20 m plot of a *Eucalyptus* plantation of each age. To ensure that all trees in the plot were scanned, a multistation scanning mode was adopted, encompassing four stations near the corners, four stations located at the middle of each boundary, and one station at the center of the plot (Figure 1c). The horizontal and vertical scanning angles of the stations were set to 0~360° and -60~90°, respectively. Reference spheres with a diameter of 14.5 cm were placed evenly in the plot for data registration. A minimum of three common spheres were needed between two adjacent stations.

UAV-LiDAR data were collected with the DJ-Innovations (DJI) Matrice M300 RTK (Shenzhen Dajiang Innovation Technology Co., Ltd., Shenzhen, China) equipped with the Zenmuse L1 laser scanning system (Figure 1a). The Zenmuse L1 integrates Livox LiDAR modules, a high-precision IMU, and a 50 inch CMOS camera on a three-axis stabilized gimbal. The flight mode was set to terrain-following mode, with a flight altitude set at 100 m above the ground surface and a speed of 10 m/s. The payload was set to triple waveform mode with a 160 kHz laser pulse emission frequency and a nonrepetitive scanning mode. The scanner was set to a ground-facing orientation of 90°. This configuration maximized the penetration of laser pulses through the canopy to the ground, resulting in high-density point cloud data.

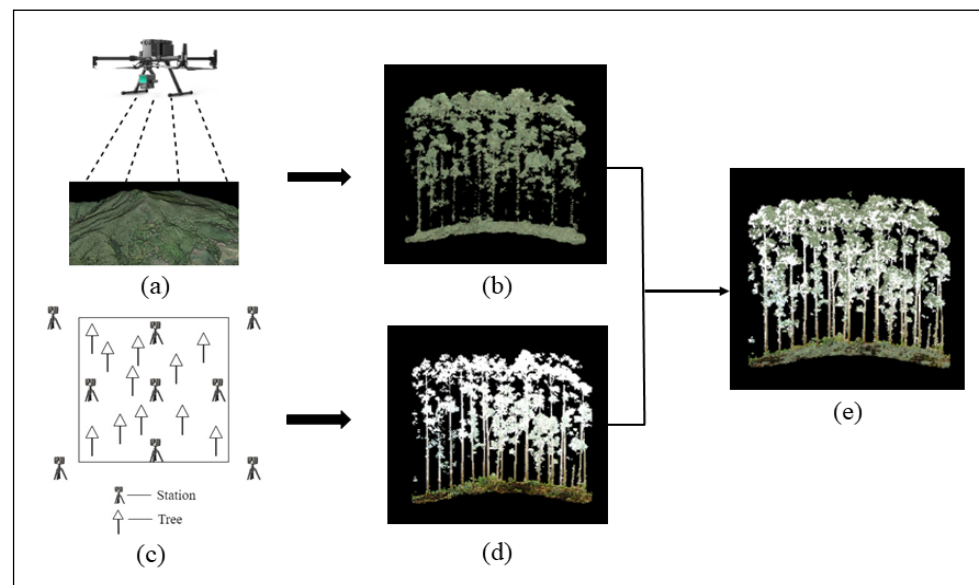


Figure 1. LiDAR data acquisition and processing. (a) UAV-LiDAR data collection process; (b) UAV-LiDAR data; (c) TLS data station setup; (d) TLS data; (e) TLS-UAV-LiDAR data.

2.3. Preprocessing of LiDAR Data

Following the acquisition of UAV-LiDAR data, a critical step involves performing differential processing using ground-synchronized global navigation satellite system (GNSS) base station data. The processed data were then imported into DJI Terra software V3.7.0 (Shenzhen Dajiang Innovation Technology Co., Ltd, Shenzhen, China) for stitching. TLS data from nine stations in each plot were stitched together using FARO SCENE software V2019.2.1 (Faro Technologies Inc., Lake Mary, FL, USA). Due to the terrestrial laser scanner using a Cartesian coordinate system, conversion was necessary based on the measured tree coordinates. UAV-LiDAR and TLS data were uniformly output in WGS-1984 coordinates and UTM projection (WGS_1984_UTM_Zone_49N). The stitched point clouds underwent further processing using LiDAR360 software V7.0 (GreenValley International Inc., Beijing, China), a robust tool for processing and analyzing LiDAR data. Potential noise at low or high altitudes in the original point cloud can be removed using algorithms based on spatial distribution.

We employed a registration approach from coarse to fine to fuse UAV-LiDAR and TLS data. Initially, point clouds sized $20\text{ m} \times 20\text{ m}$ were cropped from UAV-LiDAR and TLS data, respectively, using the coordinates of corner points measured in the field. The difference in the digital elevation model (DEM) generated from UAV-LiDAR and TLS point clouds was calculated to assess whether significant differences existed. The DEM difference was calculated as follows:

$$\text{DEM}_{\text{diff}} = \text{DEM}_{\text{UAV-LiDAR}} - \text{DEM}_{\text{TLS}} \quad (1)$$

In Equation (1), $\text{DEM}_{\text{UAV-LiDAR}}$ is the DEM generated from UAV-LiDAR data, and DEM_{TLS} is the DEM generated from TLS data. If a significant difference (DEM_{diff}) exists, adjustments can be made in LiDAR360 based on this value. This step completes the coarse registration of the point clouds between UAV-LiDAR and TLS.

We then applied the iterative closest point (ICP) algorithm [34] for fine registration of point clouds. The basic principle of ICP is based on the least-squares method, representing an optimal registration technique. It achieves this by iteratively selecting corresponding point pairs between the target point cloud (UAV-LiDAR) and the reference point cloud (TLS). The optimal iterative transformation matrix was computed through this process, and the matrix was then applied to the target point cloud. Finally, the DEM_{diff} was calculated, yielding an average DEM_{diff} of 0.008 m across all plots. The registration error root mean

square (RMS) between point clouds was 0.02 m. Given that the average point spacing in TLS was 0.08 m, this fine registration outcome met the usage requirements [35]. The point cloud fused from UAV-LiDAR and TLS is shown in Figure 1e.

2.4. Point Cloud Filtering Algorithm

2.4.1. The IPTD Algorithm

The progressive TIN densification (PTD) algorithm proposed by Axelsson [36] was initially one of the most commonly used filtering algorithms. This algorithm constructs an initial TIN model based on the initial ground points and iteratively densifies these ground points. As shown in Figure 2a, the classification of point O into ground or nonground point was determined based on two factors. The first was the perpendicular distance of the unclassified point O to the triangle ABC of the TIN. The second was the angle between point O and the vertices of triangle ABC. If point O was classified as a ground point, it was then added to the TIN. This process was repeated until all ground points were classified.

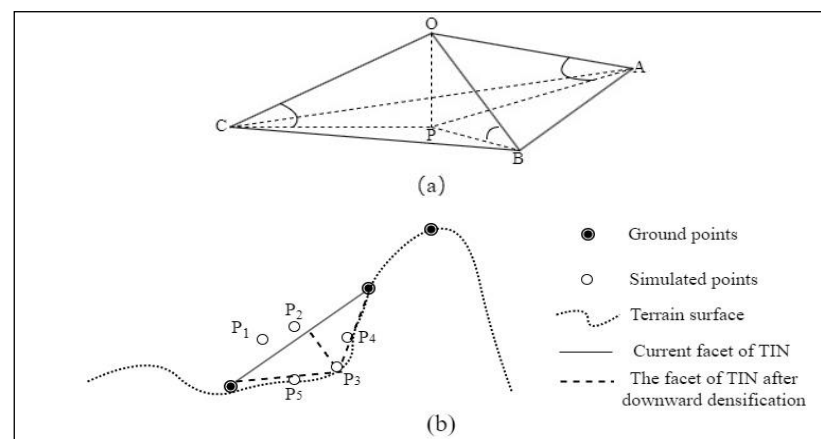


Figure 2. Schematic Diagram of IPTD Algorithm Principles. (a) The iterative densification process of TIN; (b) simple demonstration of downward densification.

However, the PTD algorithm tends to flatten the terrain in steep slope areas [37]. To better preserve terrain features, the IPTD algorithm proposed by Zhao et al. [29] improves the PTD algorithm in aspects such as seed point selection, TIN quality, and iteration order. This algorithm first uses morphological opening to obtain uniformly distributed ground seed points, overcoming the problem of uneven or insufficient seed point distribution in traditional methods, and accelerating the overall filtering speed. After constructing the initial TIN model, the PTD algorithm directly performs upward densification. In contrast, the IPTD algorithm performs downward densification before upward densification, allowing for a more detailed preservation of the characteristics of steep terrain in forested areas.

As shown in Figure 2b, points P1 and P2, near the TIN facet, will be added to densify the TIN. However, points P3, P4, and P5 on the terrain surface, due to their greater distance, will not be identified as ground points. Following downward densification, point P3, with the maximum perpendicular distance to the TIN triangle facet, is classified as a ground point and added to update the TIN. In the process of upward densification, points P4 and P5 are highly likely to be identified as ground points.

2.4.2. The CSF Algorithm

The principle of CSF is to invert the initial point clouds and cover them with a simulated cloth [38]. The simulated cloth gradually descends due to gravity. During the descent of the simulated cloth, an iterative analysis is performed to find the best corresponding points, and determine the simulated shape of the cloth that best fits the terrain (Figure 3a).

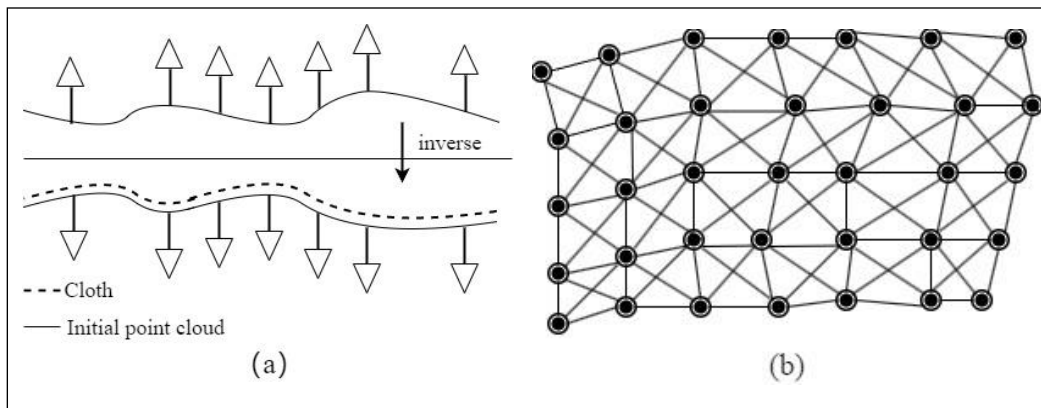


Figure 3. Schematic Diagram of CSF Algorithm Principles. (a) Cloth simulation process; (b) mass-spring model, where each circle indicates a particle and each line represents a spring.

A cloth is a grid composed of particles with constant mass interconnected by virtual springs, as illustrated in Figure 3b. This form is known as the mass-spring model [39]. In this model, the position of cloth particles in three-dimensional space determines the cloth's position and shape. To simulate the shape of the cloth at a specific time, it is necessary to calculate the positions of cloth particles in three-dimensional space. According to Newton's Second Law, the relationship between the position of cloth particles and the applied forces follows the formula below [38]:

$$X(t + \Delta t) = 2X(t) - X(t - \Delta t) + \frac{G}{m}\Delta t^2 \quad (2)$$

In Equation (2), m is the mass of cloth particles, typically set to 1; G is gravity, a known constant; X is the node position at time t ; Δt is the time step; $X(t + \Delta t)$ and $X(t - \Delta t)$ are the positions of the next and previous nodes, respectively. Given the time step and initial positions, the current position of cloth particles can be calculated.

In the cloth simulation process, the first step involves calculating the position of cloth particles after experiencing displacement due to the gravitational force, as given by Equation (2). To restrict the movement of cloth particles in the gaps of an inverted surface, it is necessary to adjust the elevation values, moving two cloth particles with different elevations to the same height. If two adjacent cloth particles are both movable points with different elevations, they move in opposite directions by the same distance. If one of the two cloth particles is immovable, the other will be moved. If these two cloth particles are at the same height, neither of them moves. The corrected displacement of cloth particles is calculated according to the following formula [38]:

$$\vec{d} = \frac{1}{2}b(\vec{p}_i - \vec{p}_0) \cdot \vec{n} \quad (3)$$

In Equation (3), \vec{d} is the displacement vector of the cloth particle; \vec{p}_0 is the current position of the designated moving cloth particle; \vec{p}_i is the position of the adjacent particle to \vec{p}_0 ; \vec{n} is the normalized vector in the vertical direction, $\vec{n} = (0, 0, 1)^T$; b is a variable used to determine whether the cloth particle is movable, where $b = 1$ when the cloth particle is movable and $b = 0$ when it is immovable.

In the traditional ground point classification process, only a single filtering algorithm (IPTD or CSF) is utilized. As shown in Figure 4, The multifiltering algorithm employed in this study included the initial application of IPTD for the classification of ground points that closely resemble the actual terrain but are relatively sparse. Then, a 0.3 m grid-sized DEM was generated through Kriging interpolation, followed by the normalization of ground points. Next, a CSF was applied for secondary filtering to densify the ground points. Upon

the completion of ground point classification, three different point cloud datasets were obtained: (1) point cloud data generated using IPTD, (2) point cloud data generated with the CSF, and (3) point cloud data generated using IPTD + CSF. We then evaluated the effects of these different point cloud datasets in individual tree parameter extraction for *Eucalyptus* plantations.

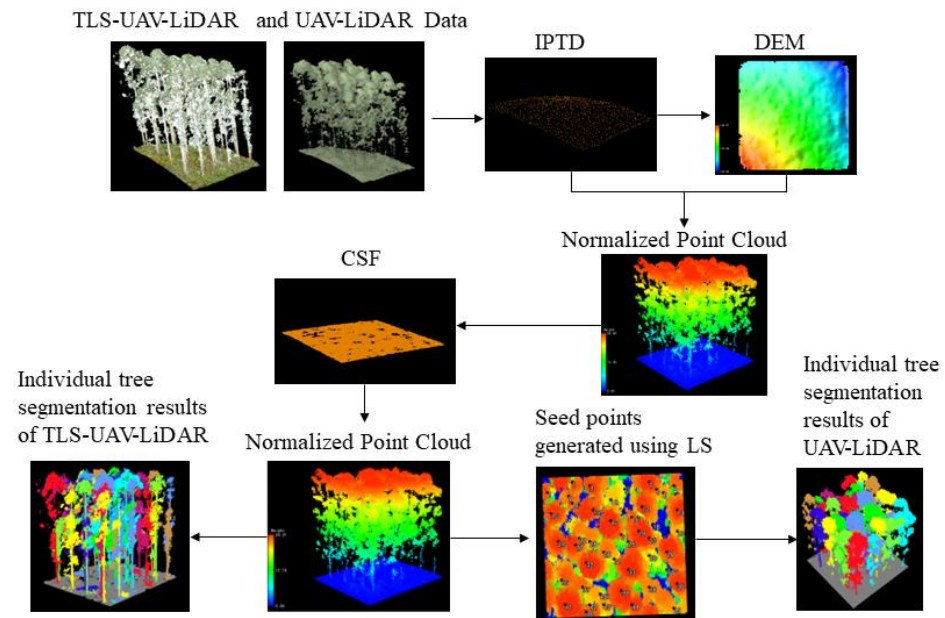


Figure 4. Schematic diagram of individual tree parameter extraction process.

2.5. Algorithm for Individual Tree Parameter Extraction

The UAV-LiDAR data are firstly used the layer stacking (LS) algorithm [40] to create seed points for individual trees positions. This algorithm divides the normalized point cloud at intervals, forming layers parallel to the ground. It applies the K-means clustering algorithm in each layer, merging the results to identify tree vertices with the highest stacking degree. Next, the point cloud segmentation (PCS) algorithm [41] segments individual trees using seed points from the LS algorithm. PCS algorithm partitions point cloud attributes based on the Euclidean distance between tree vertices, sequentially iterating from top to bottom to segment individual trees [42].

For TLS and UAV-LiDAR data, a continuous topological structure is constructed from the base to the top of the trees. This method includes two main steps: trunk detection and canopy segmentation. First, the density-based spatial clustering of applications with noise (DBSCAN) algorithm [43] was used to automatically detect the trunks and obtain the DBH at a height of 1.2~1.4 m for each tree. Then, the comparative shortest-path (CSP) algorithm [44] was used to achieve the segmentation of the tree canopy point clouds. Guided by ecological metabolic theory, the CSP algorithm determines the target tree for each point by finding the shortest distance from the point to the trunk.

2.6. Accuracy Evaluation

We evaluated the accuracy of individual tree parameter extraction according to the following two aspects: position detection rate and parameter extraction accuracy [35]. The detection rate was determined by establishing a buffer zone with the true coordinates of the trees as the center. Segmented trees falling within this buffer zone were considered correctly matched. The setting of the buffer zone's radius can be guided by the mean crown width of the trees [45]. Additionally, it can be adjusted based on the distance between the position obtained in the cloud and the equivalent position obtained on the ground. Therefore, the radius of the UAV-LiDAR buffer zone was set to 1.3 m, and the radius for

TLS and TLS-UAV-LiDAR buffer zones was set to 1 m. The detection rate was calculated as follows:

$$P = \frac{\sum_{i=1}^n n_i}{n} \times 100 \quad (4)$$

where P is the detection rate of individual trees, n_i is the number of correctly identified trees, and n the total number of trees in the measured plot.

The accuracy of parameter extraction was assessed based on tenfold cross-validation, which involves repeated random training and the validation of correctly matched trees. The precision evaluation indicators included the coefficient of determination (R^2), root mean squared error (RMSE), mean absolute deviation (MAD), and mean absolute percentage error (MAPE). The corresponding formulas are as follows:

$$R^2 = 1 - \frac{\sum_{i=1}^n (y_i - \hat{y}_i)^2}{\sum_{i=1}^n (y_i - \bar{y})^2} \quad (5)$$

$$\text{RMSE} = \sqrt{\frac{1}{n} \sum_{i=1}^n (y_i - \hat{y}_i)^2} \quad (6)$$

$$\text{MAD} = \frac{1}{n} \sum_{i=1}^n |y_i - \hat{y}_i| \quad (7)$$

$$\text{MAPE} = \frac{1}{n} \sum_{i=1}^n \left| \frac{y_i - \hat{y}_i}{y_i} \right| \times 100 \quad (8)$$

In Equations (5)–(8), \hat{y}_i represents the estimated value of an individual tree parameter extracted from LiDAR data, y_i is the measured value, \bar{y} represents the mean measured value, and n is the number of samples.

3. Results

3.1. Individual Tree Position Detection Rate

The positional matching accuracy achieved with TLS and TLS-UAV-LiDAR data was significantly higher than that obtained with UAV-LiDAR data, with detection rates reaching over 90% (Table 1). The detection rates of ULS were all below 60%, which is mainly attributed to the limitations of ULS in scanning the lower portions of canopies. As shown in Figure 5, since TLS data hold a significant advantage in terms of the position detection rate, fusing them with UAV-LiDAR data can enhance the accuracy of tree position detection compared to that achieved using ULS data alone. In contrast, the impact of filtering algorithms on the accuracy of tree position detection was not particularly significant. Therefore, the accuracy of tree detection is primarily influenced by the choice of the LiDAR data collection platform.

Table 1. Individual tree position detection rate.

LiDAR Data	Single Filtering (IPTD)		Single Filtering (CSF)		Multifiltering (IPTD + CSF)	
	Matching Tree	Detection Rate	Matching Tree	Detection Rate	Matching Tree	Detection Rate
UAV-LiDAR	178	58%	182	59%	182	59%
TLS	283	92%	283	92%	282	92%
TLS-UAV-LiDAR	274	90%	277	90%	283	92%

3.2. Individual Tree Parameter Extraction

The extraction accuracy achieved with UAV-LiDAR, TLS, and TLS-UAV-LiDAR data generally demonstrates an upward trend (Table 2). As the point cloud information became more detailed, the R^2 values for the individual tree parameter extraction increased, and the corresponding RMSE, MAD, and MAPE values decreased successively. This indicates

the limitations in using single-source LiDAR data (TLS or UAV-LiDAR) for tree height and DBH extraction. The fusion of UAV-LiDAR and TLS data can compensate for the missing trunk and canopy information, leading to a more complete representation of tree structure and enhanced accuracy in individual tree parameter extraction.

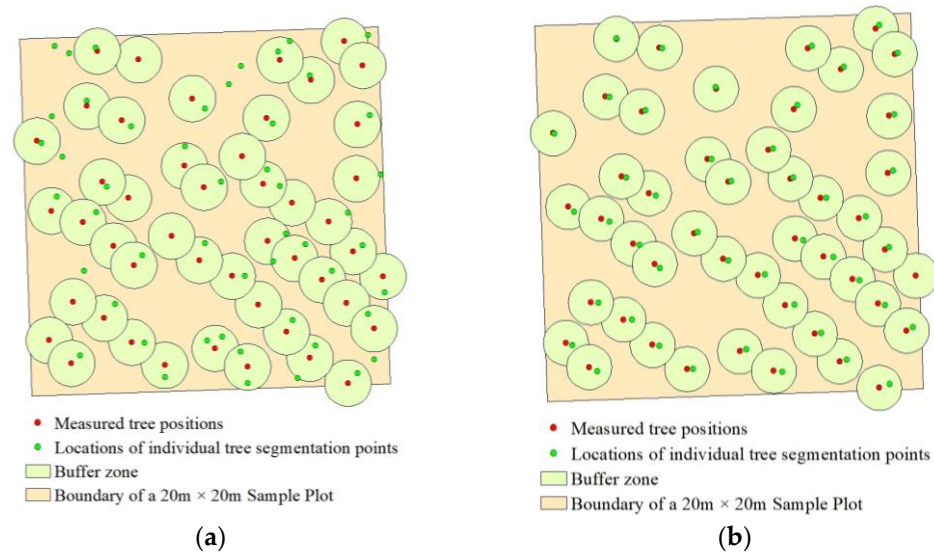


Figure 5. Individual tree position matching diagram. (a) Comparison between measured tree positions and segmented tree positions in UAV-LiDAR data; (b) comparison between measured tree positions and segmented tree positions in TLS-UAV-LiDAR data.

Table 2. The accuracy of individual tree parameter extraction.

Filter Algorithm	Structural Parameter	Evaluation Index	UAV-LiDAR	TLS	TLS-UAV-LiDAR
Single filtering (IPTD)	Tree height	R^2	0.84	0.85	0.87
		RMSE	1.91	1.76	1.63
		MAD	1.40	1.28	1.23
		MAPE	10%	9%	8%
	DBH	R^2		0.81	0.80
		RMSE		1.45	1.49
		MAD		1.10	1.14
		MAPE		10%	10%
Single filtering (CSF)	Tree height	R^2	0.82	0.82	0.84
		RMSE	2.06	1.89	1.76
		MAD	1.56	1.44	1.29
		MAPE	11%	10%	9%
	DBH	R^2		0.75	0.83
		RMSE		1.66	1.36
		MAD		1.27	1.03
		MAPE		12%	10%
Multifiltering (IPTD + CSF)	Tree height	R^2	0.85	0.89	0.89
		RMSE	1.83	1.52	1.51
		MAD	1.40	1.09	1.08
		MAPE	10%	7%	7%
	DBH	R^2		0.85	0.89
		RMSE		1.30	1.14
		MAD		1.00	0.87
		MAPE		9%	8%

Using a multifiltering algorithm can enhance the accuracy of individual tree parameter extraction from different types of LiDAR data. Compared to a single filtering algorithm (IPTD, CSF), IPTD + CSF improves the accuracy of tree height extraction. As shown in Table 2, for UAV-LiDAR data, IPTD + CSF ($R^2 = 0.85$) exhibited a 0.01 increase in R^2 compared to IPTD (0.84) and a 0.03 increase compared to CSF (0.82). For TLS data, IPTD + CSF ($R^2 = 0.89$) demonstrated a 0.04 increase in R^2 compared to IPTD (0.85) and a 0.07 increase compared to CSF (0.82). For TLS-UAV-LiDAR data, IPTD + CSF ($R^2 = 0.89$) showed a 0.02 increase in R^2 compared to IPTD (0.87) and a 0.05 increase compared to CSF (0.84). IPTD + CSF also improved the accuracy of DBH extraction with TLS and TLS-UAV-LiDAR data.

Compared to IPTD and the CSF, IPTD + CSF yielded the best results for individual tree parameter extraction with TLS-UAV-LiDAR data, correctly matching 283 trees. The extraction accuracy for both tree height and DBH reached the highest R^2 value of 0.89, with the corresponding values for RMSE, MAD, and MAPE being the lowest (Figure 6).

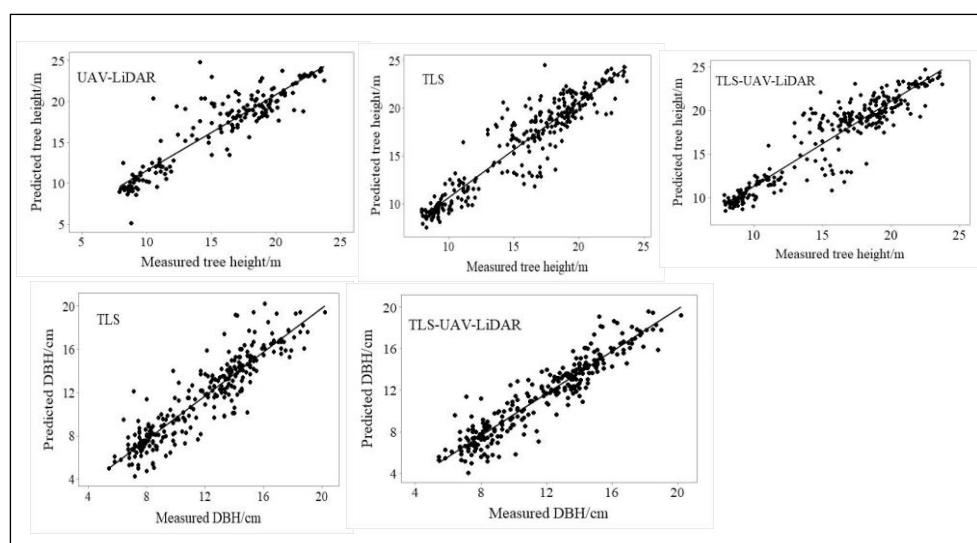


Figure 6. Performance of IPTD + CSF in extracting individual tree parameters with multiplatform LiDAR data.

4. Discussion

4.1. The Impact of Multiplatform LiDAR Data on Individual Tree Parameter Extraction

TLS has a significant advantage in depicting understory vegetation information [46]. However, due to the occlusion of branches and undergrowth, the point cloud density at the top of trees scanned using TLS is low in some cases [47]. In contrast, the UAV-LiDAR top-down scanning approach can provide detailed information about tree canopy structures. However, the laser penetration rate is weak for this scanning approach, which makes it difficult to fully capture trunk information [48]. The fusion of TLS and UAV-LiDAR data can overcome these disadvantages. Our findings indicate that TLS-UAV-LiDAR can provide more complete tree information and increase the accuracy of individual tree parameter extraction compared to using TLS or UAV-LiDAR data alone. Terryn et al. [49] also suggested that fusing TLS and UAV-LiDAR effectively improved quantifications of a tropical forest structure.

The fusion of TLS and UAV-LiDAR improves the estimation for some of the forest parameters, but may not significantly impact individual tree detection. This is mainly because TLS can comprehensively capture tree trunk information [50,51], enabling accurate matching with measured tree positions. However, the process of obtaining TLS data requires significant amounts of time and labor [52]. UAV-LiDAR supports large-scale forest investigations [53]. The fusion of TLS and UAV-LiDAR can reduce the cost of obtaining field data and enables more efficient forest inventories to be obtained. Therefore, we suggest

that the fusion of a few stations of TLS data with easily obtainable large-scale UAV-LiDAR data would improve the detection rate of individual trees and facilitate the high-precision estimation of individual tree parameters at large scales.

4.2. The Impact of Different Filtering Algorithms on the Accuracy of Individual Tree Parameter Extraction

The iterative densification process of IPTD from bottom to top enhances its capability to handle changes in slope, enabling it to effectively address various terrains and complex environments [29]. While the CSF demonstrates excellent performance in classifying ground points in flat areas, the filtering accuracy diminishes in regions characterized by a mixture of complex and flat terrains [54]. Our findings suggest that IPTD yields better results in tree height and DBH extraction with TLS data than the CSF approach. Wang et al. [55] found that filtering algorithms have different impacts on individual tree parameter extraction in forest areas using LiDAR data. For the accurate extraction of individual tree parameters, the combination of point cloud filtering algorithms is essential. IPTD + CSF not only enhances the accuracy of individual tree parameter extraction for a specific LiDAR dataset but also results in comprehensive improvements for UAV-LiDAR, TLS, and TLS-UAV-LiDAR.

The combination of different filtering algorithms can be adapted to complex environments, thus enhancing the applicability of multifiltering algorithms. Previous research also found that the use of a CSF to obtain an initial digital terrain model, followed by progressive TIN densification (PTD) for refinement, can aid in accurately distinguishing ground and nonground points in LiDAR data [30]. Wang [56] found that using morphological techniques to obtain initial ground points, followed by a secondary CSF-based filtering step, can effectively remove nonground points while retaining detailed ground features. Therefore, we recommend employing a multifiltering algorithm to separate ground points for individual tree parameter extraction with high-density LiDAR data.

5. Conclusions

This research focuses on how to increase the accuracy of individual tree parameter extraction using single- and multifilter algorithms based on TLS, UAV-LiDAR, and TLS-UAV-LiDAR data. The fusion of TLS and UAV-LiDAR can compensate for missing crown information in TLS and absent stem information in UAV-LiDAR and improve the accuracy of individual tree parameter extraction. However, when the complementary effects of TLS and UAV-LiDAR are limited, the difference in accuracy of individual tree parameter extraction before and after the fusion of TLS and UAV-LiDAR is not significant.

Our results indicate that choosing an appropriate ground point filtering algorithm is crucial before using multiplatform LiDAR data for individual tree parameter extraction. Compared to single-filtering algorithms, multifiltering algorithms are more adaptable and can improve the accuracy of individual tree parameter extraction for TLS, UAV-LiDAR, and TLS-UAV-LiDAR data, facilitating the precise quantification of the three-dimensional forest structure. As the demand for high-quality forest vegetation surveys using LiDAR technology continues to increase, we recommend using a multifiltering algorithm in combination with fused LiDAR data to enhance the accuracy of individual tree parameter extraction.

Due to the expanded possibilities offered by fused LiDAR data, which extend the capacity to capture three-dimensional forest structure characteristics, future research initiatives could focus on evaluating the complementarity of TLS and UAV-LiDAR. This will increase their applicability in forest management. Furthermore, considering the limited application of LiDAR in complex primary forests, further research could harness LiDAR for comprehensive investigations into the structure of these intricate ecosystems.

Author Contributions: Conceptualization, Y.Y., W.H. and J.H.; data curation, J.H.; funding acquisition, Y.Y. and W.H.; investigation, W.H. and J.H.; methodology, Y.Y., W.H. and J.H.; writing—original draft, J.H.; writing—review and editing, W.H. and Y.Y. All authors have read and agreed to the published version of the manuscript.

Funding: This research was supported by the National Natural Science Foundation of China (NNSFC, No. 32060369), the Key Research and Development Program of Guangxi (No. GuikeAB22035060), the NNSFC (No. 32071540), the Basic Research Fund of the Guangxi Academy of Sciences (No. CQZ-D-1904), the Basic Research Fund of Guangxi Institute of Botany (GUI ZHIYE 23005), and the Fund of the Guangxi Key Laboratory of Plant Conservation and Restoration Ecology in Karst Terrain (No. 22-035-26).

Data Availability Statement: The data presented in this study are available on request from the corresponding author. The data are not publicly available due to them also being necessary for use in future research.

Acknowledgments: We thank the Guangxi Huangmian State Owned Forest Farm for supporting the field experiments. In addition, we sincerely thank the editor and reviewers for their valuable comments and suggestions to improve the quality of this paper.

Conflicts of Interest: The authors declare no conflicts of interest.

References

1. Silveira, E.M.O.; Radeloff, V.C.; Martinuzzi, S.; Pastur, G.J.M.; Bono, J.; Politi, N.; Lizarraga, L.; Rivera, L.O.; Ciuffoli, L.; Rosas, Y.M. Nationwide native forest structure maps for Argentina based on forest inventory data, SAR Sentinel-1 and vegetation metrics from Sentinel-2 imagery. *Remote Sens. Environ.* **2023**, *285*, 113391. [[CrossRef](#)]
2. Zhao, Y.; Im, J.; Zhen, Z.; Zhao, Y. Towards accurate individual tree parameters estimation in dense forest: Optimized coarse-to-fine algorithms for registering UAV and terrestrial LiDAR data. *GIScience Remote Sens.* **2023**, *60*, 2197281. [[CrossRef](#)]
3. White, J.C.; Coops, N.C.; Wulder, M.A.; Vastaranta, M.; Hilker, T.; Tompalski, P. Remote sensing technologies for enhancing forest inventories: A review. *Can. J. Remote Sens.* **2016**, *42*, 619–641. [[CrossRef](#)]
4. Guan, H.; Su, Y.; Hu, T.; Wang, R.; Ma, Q.; Yang, Q.; Sun, X.; Li, Y.; Jin, S.; Zhang, J. A novel framework to automatically fuse multiplatform LiDAR data in forest environments based on tree locations. *IEEE Trans. Geosci. Remote Sens.* **2019**, *58*, 2165–2177. [[CrossRef](#)]
5. Novotny, J.; Navratilova, B.; Albert, J.; Cienciala, E.; Fajmon, L.; Brovkina, O. Comparison of spruce and beech tree attributes from field data, airborne and terrestrial laser scanning using manual and automatic methods. *Remote Sens. Appl. Soc. Environ.* **2021**, *23*, 100574. [[CrossRef](#)]
6. Choi, H.; Song, Y. Comparing tree structures derived among airborne, terrestrial and mobile LiDAR systems in urban parks. *GIScience Remote Sens.* **2022**, *59*, 843–860. [[CrossRef](#)]
7. Itakura, K.; Miyatani, S.; Hosoi, F. Estimating tree structural parameters via automatic tree segmentation from LiDAR point cloud data. *IEEE J. Sel. Top. Appl. Earth Obs. Remote Sens.* **2021**, *15*, 555–564. [[CrossRef](#)]
8. Brede, B.; Terry, L.; Barbier, N.; Bartholomeus, H.M.; Bartolo, R.; Calders, K.; Derroire, G.; Moorthy, S.M.K.; Lau, A.; Levick, S.R. Non-destructive estimation of individual tree biomass: Allometric models, terrestrial and UAV laser scanning. *Remote Sens. Environ.* **2022**, *280*, 113180. [[CrossRef](#)]
9. Xu, D.; Wang, H.; Xu, W.; Luan, Z.; Xu, X. LiDAR applications to estimate forest biomass at individual tree scale: Opportunities, challenges and future perspectives. *Forests* **2021**, *12*, 550. [[CrossRef](#)]
10. Harris, C.M.; Herata, H.; Hertel, F. Environmental guidelines for operation of Remotely Piloted Aircraft Systems (RPAS): Experience from Antarctica. *Biol. Conserv.* **2019**, *236*, 521–531. [[CrossRef](#)]
11. Balsi, M.; Esposito, S.; Fallavollita, P.; Nardinocchi, C. Single-tree detection in high-density LiDAR data from UAV-based survey. *Eur. J. Remote Sens.* **2018**, *51*, 679–692. [[CrossRef](#)]
12. Brede, B.; Calders, K.; Lau, A.; Raunonen, P.; Bartholomeus, H.M.; Herold, M.; Kooistra, L. Non-destructive tree volume estimation through quantitative structure modelling: Comparing UAV laser scanning with terrestrial LIDAR. *Remote Sens. Environ.* **2019**, *233*, 111355. [[CrossRef](#)]
13. Disney, M.I.; Boni Vicari, M.; Burt, A.; Calders, K.; Lewis, S.L.; Raunonen, P.; Wilkes, P. Weighing trees with lasers: Advances, challenges and opportunities. *Interface Focus* **2018**, *8*, 20170048. [[CrossRef](#)]
14. Xu, D.; Chen, G.; Zhang, S.; Jing, W. An Automated Pipeline for Extracting Forest Structural Parameters by Integrating UAV and Ground-Based LiDAR Point Clouds. *Forests* **2023**, *14*, 2179. [[CrossRef](#)]
15. Demol, M.; Verbeeck, H.; Gielen, B.; Armston, J.; Burt, A.; Disney, M.; Duncanson, L.; Hackenberg, J.; Kükenbrink, D.; Lau, A. Estimating forest above-ground biomass with terrestrial laser scanning: Current status and future directions. *Methods Ecol. Evol.* **2022**, *13*, 1628–1639. [[CrossRef](#)]
16. Liu, L.X.; Pang, Y.; Li, Z.Y. Individual Tree DBH and Height Estimation Using Terrestrial Laser Scanning (TLS) in A Subtropical Forest. *Sci. Silvae Sin.* **2016**, *52*, 26–37.
17. Lin, Y.-C.; Shao, J.; Shin, S.-Y.; Saka, Z.; Joseph, M.; Manish, R.; Fei, S.; Habib, A. Comparative analysis of multi-platform, multi-resolution, multi-temporal LiDAR data for forest inventory. *Remote Sens.* **2022**, *14*, 649. [[CrossRef](#)]
18. Chen, C.; Zhou, L.; Li, X.; Zhao, Y.; Yu, J.; Lv, L.; Du, H. Optimizing the Spatial Structure of Metasequoia Plantation Forest Based on UAV-LiDAR and Backpack-LiDAR. *Remote Sens.* **2023**, *15*, 4090. [[CrossRef](#)]

19. Fekry, R.; Yao, W.; Cao, L.; Shen, X. Ground-based/UAV-LiDAR data fusion for quantitative structure modeling and tree parameter retrieval in subtropical planted forest. *For. Ecosyst.* **2022**, *9*, 100065. [[CrossRef](#)]
20. Panagiotidis, D.; Abdollahnejad, A.; Slavik, M. 3D point cloud fusion from UAV and TLS to assess temperate managed forest structures. *Int. J. Appl. Earth Obs. Geoinf.* **2022**, *112*, 102917. [[CrossRef](#)]
21. Yan, W.; Guan, H.; Cao, L.; Yu, Y.; Gao, S.; Lu, J. An automated hierarchical approach for three-dimensional segmentation of single trees using UAV LiDAR data. *Remote Sens.* **2018**, *10*, 1999. [[CrossRef](#)]
22. Liu, L.; Lim, S.; Shen, X.; Yebra, M. A hybrid method for segmenting individual trees from airborne lidar data. *Comput. Electron. Agric.* **2019**, *163*, 104871. [[CrossRef](#)]
23. Cai, Z.; Ma, H.; Zhang, L. Feature selection for airborne LiDAR data filtering: A mutual information method with Parzon window optimization. *GIScience Remote Sens.* **2020**, *57*, 323–337. [[CrossRef](#)]
24. Li, H.; Ye, C.; Guo, Z.; Wei, R.; Wang, L.; Li, J. A fast progressive TIN densification filtering algorithm for airborne LiDAR data using adjacent surface information. *IEEE J. Sel. Top. Appl. Earth Obs. Remote Sens.* **2021**, *14*, 12492–12503. [[CrossRef](#)]
25. Klápště, P.; Fogl, M.; Barták, V.; Gdulová, K.; Urban, R.; Moudrý, V. Sensitivity analysis of parameters and contrasting performance of ground filtering algorithms with UAV photogrammetry-based and LiDAR point clouds. *Int. J. Digit. Earth* **2020**, *13*, 1672–1694. [[CrossRef](#)]
26. Rashidi, P.; Rastiveis, H. Ground filtering LiDAR data based on multi-scale analysis of height difference threshold. *Int. Arch. Photogramm. Remote Sens. Spat. Inf. Sci.* **2017**, *42*, 225–229. [[CrossRef](#)]
27. Zhao, X.; Su, Y.; Li, W.; Hu, T.; Liu, J.; Guo, Q. A comparison of LiDAR filtering algorithms in vegetated mountain areas. *Can. J. Remote Sens.* **2018**, *44*, 287–298. [[CrossRef](#)]
28. Zeybek, M.; Şanlıoğlu, İ. Point cloud filtering on UAV based point cloud. *Measurement* **2019**, *133*, 99–111. [[CrossRef](#)]
29. Zhao, X.; Guo, Q.; Su, Y.; Xue, B. Improved progressive TIN densification filtering algorithm for airborne LiDAR data in forested areas. *ISPRS J. Photogramm. Remote Sens.* **2016**, *117*, 79–91. [[CrossRef](#)]
30. Cai, S.; Zhang, W.; Liang, X.; Wan, P.; Qi, J.; Yu, S.; Yan, G.; Shao, J. Filtering airborne LiDAR data through complementary cloth simulation and progressive TIN densification filters. *Remote Sens.* **2019**, *11*, 1037. [[CrossRef](#)]
31. Leite, R.V.; Silva, C.A.; Mohan, M.; Cardil, A.; Almeida, D.R.A.d.; Carvalho, S.d.P.C.e.; Jaafar, W.S.W.M.; Guerra-Hernández, J.; Weiskittel, A.; Hudak, A.T. Individual tree attribute estimation and uniformity assessment in fast-growing *Eucalyptus* Spp. forest plantations using Lidar and linear mixed-effects models. *Remote Sens.* **2020**, *12*, 3599. [[CrossRef](#)]
32. Yao, Y.; Huang, J.; He, W.; Zhu, J.; Li, Y. Changes in Water-Use Efficiency of Eucalyptus Plantations and Its Driving Factors in a Small County in South China. *Water* **2023**, *15*, 2754. [[CrossRef](#)]
33. Almeida, D.R.A.d.; Broadbent, E.N.; Zambrano, A.M.A.; Wilkinson, B.E.; Ferreira, M.E.; Chazdon, R.; Meli, P.; Gorgens, E.B.; Silva, C.A.; Stark, S.C. Monitoring the structure of forest restoration plantations with a drone-lidar system. *Int. J. Appl. Earth Obs. Geoinf.* **2019**, *79*, 192–198. [[CrossRef](#)]
34. Gressin, A.; Mallet, C.; Demantké, J.; David, N. Towards 3D lidar point cloud registration improvement using optimal neighborhood knowledge. *ISPRS J. Photogramm. Remote Sens.* **2013**, *79*, 240–251. [[CrossRef](#)]
35. Zhu, J.F.; Liu, Q.W.; Cui, X.M.; Zhang, W.B. Extraction of individual tree parameters by combining terrestrial and UAV LiDAR. *Trans. Chin. Soc. Agric. Eng.* **2022**, *38*, 51–58.
36. Axelsson, P. DEM generation from laser scanner data using adaptive TIN models. *Int. Arch. Photogramm. Remote Sens.* **2000**, *33*, 110–117.
37. Zhang, J.; Lin, X. Filtering airborne LiDAR data by embedding smoothness-constrained segmentation in progressive TIN densification. *ISPRS J. Photogramm. Remote Sens.* **2013**, *81*, 44–59. [[CrossRef](#)]
38. Zhang, W.; Qi, J.; Wan, P.; Wang, H.; Xie, D.; Wang, X.; Yan, G. An easy-to-use airborne LiDAR data filtering method based on cloth simulation. *Remote Sens.* **2016**, *8*, 501. [[CrossRef](#)]
39. Provot, X. Deformation constraints in a mass-spring model to describe rigid cloth behaviour. In *Graphics Interface*; Canadian Information Processing Society: Mississauga, ON, Canada, 1995.
40. Ayrey, E.; Fraver, S.; Kershaw, J.A., Jr.; Kenefic, L.S.; Hayes, D.; Weiskittel, A.R.; Roth, B.E. Layer stacking: A novel algorithm for individual forest tree segmentation from LiDAR point clouds. *Can. J. Remote Sens.* **2017**, *43*, 16–27. [[CrossRef](#)]
41. Li, W.; Guo, Q.; Jakubowski, M.K.; Kelly, M. A new method for segmenting individual trees from the lidar point cloud. *Photogramm. Eng. Remote Sens.* **2012**, *78*, 75–84. [[CrossRef](#)]
42. Ma, K.; Chen, Z.; Fu, L.; Tian, W.; Jiang, F.; Yi, J.; Du, Z.; Sun, H. Performance and sensitivity of individual tree segmentation methods for UAV-LiDAR in multiple forest types. *Remote Sens.* **2022**, *14*, 298. [[CrossRef](#)]
43. Pu, Y.; Xu, D.; Wang, H.; Li, X.; Xu, X. A New Strategy for Individual Tree Detection and Segmentation from Leaf-on and Leaf-off UAV-LiDAR Point Clouds Based on Automatic Detection of Seed Points. *Remote Sens.* **2023**, *15*, 1619. [[CrossRef](#)]
44. Tao, S.; Wu, F.; Guo, Q.; Wang, Y.; Li, W.; Xue, B.; Hu, X.; Li, P.; Tian, D.; Li, C. Segmenting tree crowns from terrestrial and mobile LiDAR data by exploring ecological theories. *ISPRS J. Photogramm. Remote Sens.* **2015**, *110*, 66–76. [[CrossRef](#)]
45. Wang, W.W.; Pang, Y.; Du, L.M.; Zhang, Z.J.; Liang, X.J. Individual tree segmentation for airborne LiDAR point cloud data using spectral clustering and supervoxel-based algorithm. *Natl. Remote Sens. Bull.* **2022**, *26*, 1650–1661. [[CrossRef](#)]
46. Yrttimaa, T.; Junttila, S.; Luoma, V.; Calders, K.; Kankare, V.; Saarinen, N.; Kukko, A.; Holopainen, M.; Hyyppä, J.; Vastaranta, M. Capturing seasonal radial growth of boreal trees with terrestrial laser scanning. *For. Ecol. Manag.* **2023**, *529*, 120733. [[CrossRef](#)]

47. Lau, A.; Martius, C.; Bartholomeus, H.; Shenkin, A.; Jackson, T.; Malhi, Y.; Herold, M.; Bentley, L.P. Estimating architecture-based metabolic scaling exponents of tropical trees using terrestrial LiDAR and 3D modelling. *For. Ecol. Manag.* **2019**, *439*, 132–145. [[CrossRef](#)]
48. Kükenbrink, D.; Schneider, F.D.; Leiterer, R.; Schaepman, M.E.; Morsdorf, F. Quantification of hidden canopy volume of airborne laser scanning data using a voxel traversal algorithm. *Remote Sens. Environ.* **2017**, *194*, 424–436. [[CrossRef](#)]
49. Terryn, L.; Calders, K.; Bartholomeus, H.; Bartolo, R.E.; Brede, B.; D’Hont, B.; Disney, M.; Herold, M.; Lau, A.; Shenkin, A. Quantifying tropical forest structure through terrestrial and UAV laser scanning fusion in Australian rainforests. *Remote Sens. Environ.* **2022**, *271*, 112912. [[CrossRef](#)]
50. Liang, X.; Kankare, V.; Hyyppä, J.; Wang, Y.; Kukko, A.; Haggrén, H.; Yu, X.; Kaartinen, H.; Jaakkola, A.; Guan, F. Terrestrial laser scanning in forest inventories. *ISPRS J. Photogramm. Remote Sens.* **2016**, *115*, 63–77. [[CrossRef](#)]
51. Yun, Z.; Zheng, G. Stratifying forest overstory and understory for 3-D segmentation using terrestrial laser scanning data. *IEEE J. Sel. Top. Appl. Earth Obs. Remote Sens.* **2021**, *14*, 12114–12131. [[CrossRef](#)]
52. Wilkes, P.; Lau, A.; Disney, M.; Calders, K.; Burt, A.; de Tanago, J.G.; Bartholomeus, H.; Brede, B.; Herold, M. Data acquisition considerations for terrestrial laser scanning of forest plots. *Remote Sens. Environ.* **2017**, *196*, 140–153. [[CrossRef](#)]
53. Bruggisser, M.; Hollaus, M.; Otepka, J.; Pfeifer, N. Influence of ULS acquisition characteristics on tree stem parameter estimation. *ISPRS J. Photogramm. Remote Sens.* **2020**, *168*, 28–40. [[CrossRef](#)]
54. Wan, P.; Zhang, W.; Skidmore, A.K.; Qi, J.; Jin, X.; Yan, G.; Wang, T. A simple terrain relief index for tuning slope-related parameters of LiDAR ground filtering algorithms. *ISPRS J. Photogramm. Remote Sens.* **2018**, *143*, 181–190. [[CrossRef](#)]
55. Wang, J.W.; Li, X.X.; Zhang, H.Q. Terrain Adaptive Filtering Method Based on Elevation Normalization. *Laser Optoelectron. Prog.* **2022**, *59*, 1028008.
56. Wang, K. Research on Point Cloud Filtering Algorithm and Feature Extraction of Airborne Lidar. Master’s Thesis, East China University of Technology, Fuzhou, China, 2021.

Disclaimer/Publisher’s Note: The statements, opinions and data contained in all publications are solely those of the individual author(s) and contributor(s) and not of MDPI and/or the editor(s). MDPI and/or the editor(s) disclaim responsibility for any injury to people or property resulting from any ideas, methods, instructions or products referred to in the content.